

ILLUMINATING A DARK LENS : A TYPE IA SUPERNOVA MAGNIFIED BY GALAXY CLUSTER ABELL 2744

STEVEN A. RODNEY^{1,2}, ET AL.

Draft version February 18, 2015

ABSTRACT

SN HFF14Tom is a Type Ia Supernova (SN Ia) discovered at $z = 1.33$ behind the galaxy cluster Abell 2744 ($z = 0.308$). This SN has a projected separation from the cluster core of $\sim 40''$, closer than any other cluster-lensed SN Ia. As such, it provides the first opportunity to confront gravitational lens models of galaxy clusters with the direct measurement of an absolute magnification at the edge of the strong-lensing region. We derive a tightly constrained measure of the peak apparent magnitude, corrected for light curve shape and extinction. In a cosmology-independent analysis, we find that HFF14Tom is 0.71 ± 0.12 magnitudes brighter than unlensed SNe Ia at similar redshift, implying a lensing magnification of $\mu_{\text{obs}} = 1.9 \pm 0.2$. Predicted magnifications from 7 independent groups are systematically biased to higher values, with a mean of $\mu_{\text{mod}} = 2.4 \pm 0.3$ and some models disagreeing by $> 6\sigma$. **TODO: summarize lensing discussion.**

Subject headings: supernovae: general

1. INTRODUCTION

Massive galaxy clusters can be used as cosmic telescopes to magnify distant background objects through gravitational lensing. This can substantially increase the reach of deep imaging surveys, and has recently been used to discover candidate proto-galaxies formed in the first Gyr after the Big Bang (Zheng et al. 2012; Coe et al. 2013) (**cite other high-z galaxy candidates discovered with lensing**)

Lensed SNe have been discovered (Goobar et al. 2009; Richm et al. 2011)

Patel et al. (2014, hereafter P14) and Nordin et al. (2014) presented independent analyses of three lensed SNe, of which at least 2 are securely classified as Type Ia SNe. All of these three objects were found in the Cluster Lensing and Supernova survey with Hubble (CLASH, PI:Postman, HST Program ID 12068).

In Section 2 we present the discovery and follow-up observations of SN HFF14Tom at $z = 1.31$, discovered behind the galaxy cluster Abell 2744. Sections 3 and 4 describe the spectroscopy and photometry of this SN, leading to a classification of the object as a normal Type Ia SN. In Section ?? we make a direct measurement of the magnification of this source due to gravitational lensing, and compare to predictions from lens models. Finally, Section ?? discusses the tension between our magnification measurement and the lens models, with implications for the systematic error budget in magnification estimates for other high- z lensed sources.

2. DISCOVERY, FOLLOW-UP, AND DATA PROCESSING

SN HFF14Tom was discovered in *HST* observations with the Advanced Camera for Surveys (ACS) in the F606W and F814W bands (V and i), collected on UT 2014 May 15 as part of the Hubble Frontier Fields (HFF) survey (PI:J.Lotz, HST-PID:13495).³ The HFF program

is a 3-year director's discretionary initiative that is collecting 140 orbits of HST imaging (roughly 340 ksec) on six massive galaxy clusters, plus 6 accompanying "parallel fields." Each field is observed in 3 optical bands (ACS F435W, F606W and F814W) and 4 infrared (IR) bands (WFC3-IR F105W, F125W, F140W, and F160W), although the optical and IR imaging campaigns are separated by ~ 6 months. Abell 2744 was the first cluster observed, with IR imaging spanning 2013 October–November, and optical imaging from 2014 May–July. A composite image of the HFF data showing the SN is presented in Figure 1. The SN detection was made in difference images constructed using template imaging of Abell 2744 from HST+ACS observations taken in 2009 (PI:Dupke, HST-PID:11689).

The most probable host galaxy for SN HFF14Tom is a faint and diffuse galaxy immediately to the south-east of the SN location. With photometry of the host galaxy collected from the template images, we fit the spectral energy distribution (SED) using the *BPZ* code – a Bayesian photometric redshift estimator (Benítez 2000). The best-fit SED template match is shown in Figure 2. From the *BPZ* analysis, we found the host to be most likely a late-type galaxy at a redshift of $z = 1.5 \pm 0.2$.

Upon discovery, HST target-of-opportunity observations were triggered from the FrontierSN program (PI:Rodney, HST-PID:13386), which aims to discover and follow transient sources in the HFF cluster and parallel fields. The FrontierSN observations provided WFC3-IR imaging as well as spectroscopy using the ACS G800L grism, supplementing the rapid-cadence optical imaging from HST+ACS already being provided by the HFF program. Difference images for the IR follow-up data were generated using templates constructed from the HFF WFC3-IR imaging campaign, which concluded in November, 2013.

All of the imaging data were processed using the `sndrizpipe` pipeline,⁴ a custom data reduction package

¹ Department of Physics and Astronomy, The Johns Hopkins University, Baltimore, MD 21218.

² Hubble fellow

³ <http://www.stsci.edu/hst/campaigns/frontier-fields>

⁴ <https://github.com/srodney/sndrizpipe> v1.2
DOI:10.5281/zenodo.10731

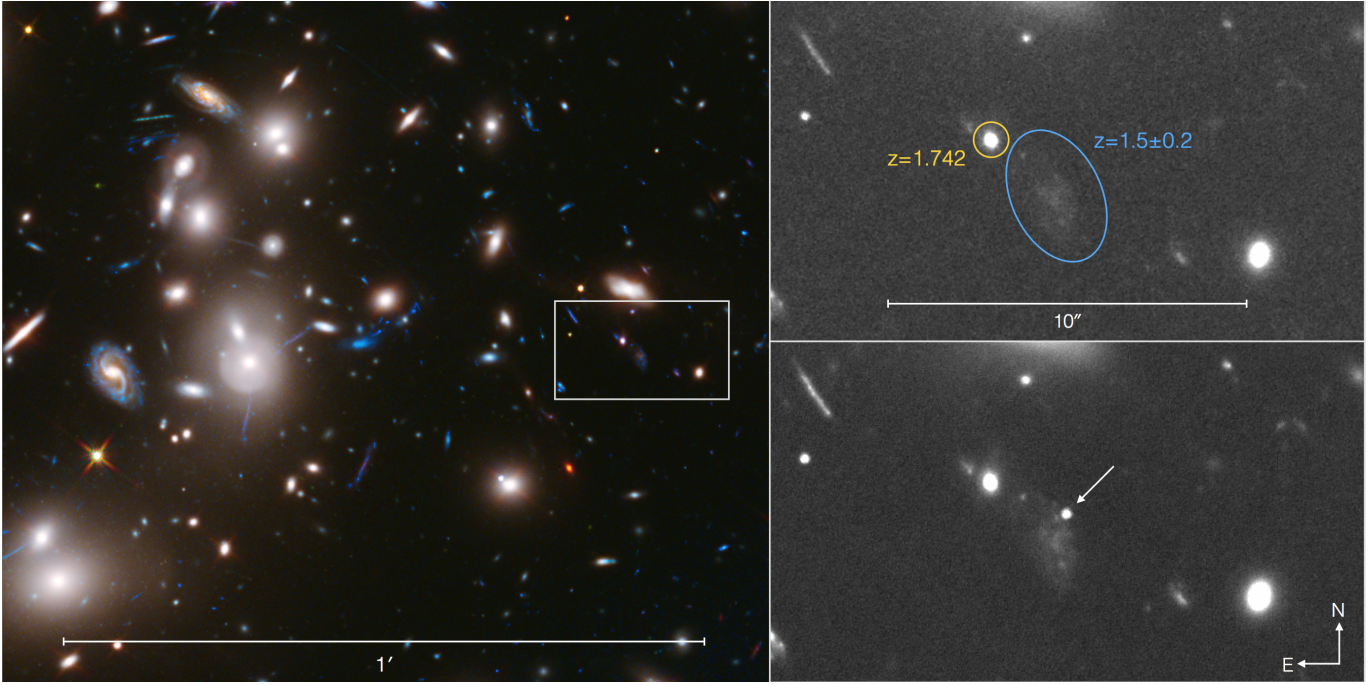


Figure 1. SN HFF14Tom in the Abell 2744 field. The left panel shows a UV/Optical/IR color composite image constructed from all available HST imaging of the Abell 2744 cluster field. The inset panels at right show F814W imaging of the immediate vicinity of SN HFF14Tom, approximately 40'' from the center of the cluster. The top panel shows the template image, combining all data prior to the SN appearance. Labeled ellipses mark the nearest galaxies and their redshift constraints: a photometric redshift for the most likely host galaxy is marked in blue, and the spectroscopic redshift for a likely background galaxy is given in yellow. The bottom panel is constructed from all HFF F814W imaging taken while the SN was detectable, and marks the SN location with an arrow. (Left panel image credit: NASA, ESA, and J. Lotz, M. Mountain, A. Koekemoer, and the HFF Team (STScI))

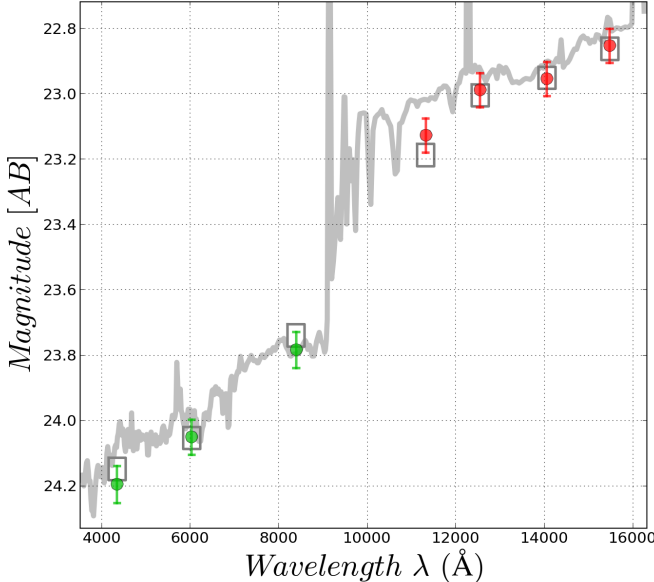


Figure 2. Best-fit SED template match for the most probable HFF14Tom host galaxy. Using the *BPZ* code to match the observed SED, we find the nearest galaxy to the SN position is a late type galaxy with a photometric redshift of $z = 1.5 \pm 0.2$.

in Python that is employs the **DrizzlePac** tools from the Space Telescope Science Institute (STScI) (Fruchter et al. 2010). Photometry was collected using the **PyPhot** software package,⁵ a pure-Python implementation of the

photometry algorithms from the IDL AstroLib package (Landsman 1993), which in turn are based on the DAOPHOT program (Stetson 1987). For the IR bands we used point spread function (PSF) fitting on the difference images, and in the ACS optical bands we collected photometry with a $0''.3$ aperture. Table 1 presents the list of observations, along with measured photometry from all available imaging data.

3. SPECTROSCOPY

A spectrum of SN HFF14Tom was collected with the ACS G800L grism on 2014 June 4 and 7, when the SN was very near to its peak brightness. The observations – listed at the bottom of Table 1 – used 5 HST orbits from the FrontierSN program for a total spectroscopic exposure time of ~ 10 ksec. The grism data were processed and the target spectrum was extracted using the custom pipeline employed by the Grism Lens Amplified Survey from Space program (GLASS; PI:Treu, PID:13459). Is there a citation for this? or more to say here?

Figure 3 shows the composite 1-D ACS grism spectrum, combining all available G800L exposures, overlaid with SN model fits that will be described below. The spectrum is largely free of contamination, because the orientation was chosen to avoid nearby bright sources and the host galaxy is diffuse and optically faint. Thus, the SN spectral features can be unambiguously identified, most notably the red slope of the continuum and a prominent absorption feature at $\sim 8700\text{\AA}$. However, the signal to noise ratio (S/N) for the host galaxy spectrum was too weak to yield any additional constraints on the host type or redshift.

⁵ <https://github.com/djones1040/PyPhot>

Table 1
HFF14Tom Observations and Photometry

Obs. Date (MJD)	Camera	Filter or grism	Exp. Time (sec)	Flux (counts/sec)	Flux Err (counts/sec)	AB Mag ^a	Mag Err	AB Zero Point	ΔZP ^b (Vega-AB)
56820.06	ACS	F435W	5083	-0.027	0.053	27.66	...	25.665	-0.102
56821.85	ACS	F435W	5083	0.105	0.053	28.11	0.55	25.665	-0.102
56823.77	ACS	F435W	5083	0.022	0.053	29.80	2.59	25.665	-0.102
56824.97	ACS	F435W	5083	0.021	0.053	29.85	2.72	25.665	-0.102
56828.68	ACS	F435W	5083	-0.148	0.053	27.65	...	25.665	-0.102
56830.87	ACS	F435W	5083	0.100	0.054	28.16	0.58	25.665	-0.102
56832.86	ACS	F435W	5083	-0.080	0.053	27.66	...	25.665	-0.102
56833.86	ACS	F435W	5083	-0.002	0.053	27.67	...	25.665	-0.102
56839.50	ACS	F435W	5083	-0.022	0.052	27.68	...	25.665	-0.102
56792.06	ACS	F606W	5046	0.363	0.083	27.59	0.25	26.493	-0.086
56792.98	ACS	F606W	3586	0.692	0.095	26.89	0.15	26.493	-0.086
56797.10	ACS	F606W	4977	0.968	0.087	26.53	0.10	26.493	-0.086
56800.08	ACS	F606W	4977	0.844	0.085	26.68	0.11	26.493	-0.086
56804.99	ACS	F606W	5046	0.977	0.086	26.52	0.10	26.493	-0.086
56792.99	ACS	F814W	3652	1.639	0.104	25.41	0.07	25.947	-0.424
56797.11	ACS	F814W	4904	3.376	0.141	24.63	0.05	25.947	-0.424
56798.95	ACS	F814W	5046	3.951	0.156	24.46	0.04	25.947	-0.424
56800.10	ACS	F814W	4904	3.854	0.155	24.48	0.04	25.947	-0.424
56801.89	ACS	F814W	10092	4.102	0.153	24.41	0.04	25.947	-0.424
56802.95	ACS	F814W	10092	4.325	0.160	24.36	0.04	25.947	-0.424
56803.93	ACS	F814W	15138	4.402	0.160	24.34	0.04	25.947	-0.424
56804.08	ACS	F814W	5046	4.658	0.178	24.28	0.04	25.947	-0.424
56812.08	ACS	F814W	637	4.705	0.258	24.27	0.06	25.947	-0.424
56815.93	ACS	F814W	446	4.026	0.285	24.43	0.08	25.947	-0.424
56820.07	ACS	F814W	5044	3.508	0.142	24.58	0.04	25.947	-0.424
56821.87	ACS	F814W	5044	3.541	0.144	24.57	0.04	25.947	-0.424
56823.79	ACS	F814W	5044	2.876	0.124	24.80	0.05	25.947	-0.424
56824.99	ACS	F814W	5044	3.060	0.129	24.73	0.05	25.947	-0.424
56828.70	ACS	F814W	5044	2.777	0.121	24.84	0.05	25.947	-0.424
56830.89	ACS	F814W	5044	2.395	0.111	25.00	0.05	25.947	-0.424
56832.88	ACS	F814W	5044	2.331	0.108	25.03	0.05	25.947	-0.424
56833.88	ACS	F814W	5044	2.389	0.111	25.00	0.05	25.947	-0.424
56839.52	ACS	F814W	5044	1.673	0.093	25.39	0.06	25.947	-0.424
56833.14	WFC3-IR	F105W	756	7.504	0.239	24.08	0.03	26.269	-0.645
56841.82	WFC3-IR	F105W	756	5.822	0.208	24.36	0.04	26.269	-0.645
56850.06	WFC3-IR	F105W	756	3.952	0.207	24.78	0.06	26.269	-0.645
56860.62	WFC3-IR	F105W	1159	2.899	0.167	25.11	0.06	26.269	-0.645
56886.63	WFC3-IR	F105W	1159	1.216	0.147	26.06	0.13	26.269	-0.645
56891.67	WFC3-IR	F105W	356	0.971	0.324	26.30	0.36	26.269	-0.645
56893.20	WFC3-IR	F105W	712	0.954	0.242	26.32	0.28	26.269	-0.645
56954.64	WFC3-IR	F105W	356	0.521	0.388	26.98	0.81	26.269	-0.645
56817.08	WFC3-IR	F125W	1206	8.459	0.191	23.91	0.02	26.230	-0.901
56833.15	WFC3-IR	F125W	756	7.753	0.255	24.01	0.04	26.230	-0.901
56841.83	WFC3-IR	F125W	806	6.015	0.227	24.28	0.04	26.230	-0.901
56850.07	WFC3-IR	F125W	806	4.343	0.224	24.64	0.06	26.230	-0.901
56891.86	WFC3-IR	F140W	712	2.578	0.344	25.42	0.14	26.452	-1.076
56893.06	WFC3-IR	F140W	712	3.026	0.363	25.25	0.13	26.452	-1.076
56955.58	WFC3-IR	F140W	1424	1.218	0.269	26.24	0.24	26.452	-1.076
56817.09	WFC3-IR	F160W	1206	4.831	0.263	24.24	0.06	25.946	-1.251
56833.21	WFC3-IR	F160W	756	3.965	0.241	24.45	0.07	25.946	-1.251
56841.84	WFC3-IR	F160W	756	3.011	0.234	24.75	0.08	25.946	-1.251
56850.08	WFC3-IR	F160W	756	2.744	0.223	24.85	0.09	25.946	-1.251
56860.67	WFC3-IR	F160W	1159	1.895	0.177	25.25	0.10	25.946	-1.251
56886.64	WFC3-IR	F160W	1159	1.677	0.191	25.38	0.12	25.946	-1.251
56812.0	ACS	G800L	3490
56815.7	ACS	G800L	6086

^a For non-positive flux values we report the magnitude as a 3- σ upper limit

^b Zero point difference: the magnitude shift for conversion from AB to Vega magnitude units.

As described below, we fit the SN HFF14Tom spectrum in two steps. First we determine a spectral classification – and get a preliminary estimate of the redshift and age – using the SuperNova IDentification (SNID) software (Blondin & Tonry 2007). Second, we refine the redshift and age measurement using a custom Type Ia spectral template matching program.

3.1. Classification with SNID

The SNID program is designed to estimate the type, redshift, and age of a SN spectrum through cross-correlation matching with a library of template spectra. To account for possible distortions in the broad shape of the SN pseudo-continuum due to dust or instrumental calibration effects, SNID divides each SED by a smooth

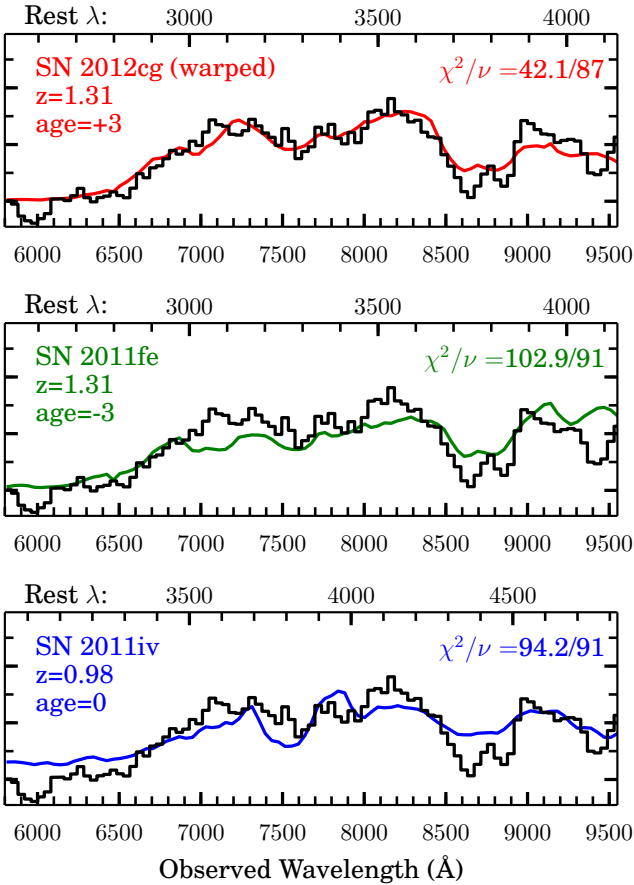


Figure 3. Redshift and age determination from spectral template matching to the the SN HFF14Tom maximum light spectrum. The y axis plots flux in arbitrary units, and the x axis marks wavelength in Å with the observer-frame on the bottom and rest-frame on the top. The HFF14Tom spectrum observed with the HST ACS G800L grism is shown in black, overlaid with model fits derived from a library of Type Ia templates that have extended rest-frame UV coverage. *Top:* The best match is at $z = 1.31$ with $\text{age} = +3$ days, from the normal Type Ia SN 2012cg template when using a smooth 3rd-order polynomial to warp the shape of the template pseudo-continuum. When the templates are not warped, an acceptable fit can be found with a normal Type Ia at $z = 1.31$ (middle) or at $z \sim 1$ (bottom), although the latter is inconsistent with the host galaxy redshift prior and the light curve. No CC SN templates can provide a statistically acceptable fit at any redshift, within the age constraints imposed by the light curve.

cubic spline fit. This effectively removes the shape of the SN pseudo-continuum to leave behind a flat SED superimposed with spectral absorption and emission features. It is these features which drive the cross-correlation fit, so the SNID approach is insensitive to the overall color of the SED. We used v2.0 of the SNID template library, which includes template SEDs covering all Type Ia and Core Collapse sub-classes, and has recently been updated with corrections and improvements to the Type Ib/c templates (Liu & Modjaz 2014).

In SNID the goodness of fit is evaluated primarily through the r_{lap} parameter, which measures the degree of wavelength overlap and the strength of the cross-correlation peak. Typically, an r_{lap} value > 5 is required to be considered an acceptable match.

To match the SN HFF14Tom spectrum we use conservative constraints on age and redshift: limiting the age to ± 5 rest-frame days of peak brightness and $0.8 < z < 1.8$, consistent with the SN light curve and host galaxy photo- z . With these constraints we find that the only acceptable match is a normal Type Ia SN near $z = 1.3$. The best match has $r_{\text{lap}} = 8.7$, using the normal Type Ia SN 2005cf at $z = 1.35$ and $\text{age} = -2.2$ rest-frame days before peak. Within these constraints, the best non-Ia matches all have $r_{\text{lap}} < 2.5$.

The SNID library can generate an acceptable CC SN match only when we remove all age and redshift constraints. In this case the best non-Ia match is the Type Ic SN 1997ef, which delivers $r_{\text{lap}} = 6.8$ at $z = 0.51$ and $\text{age} = 47.3$ rest-frame days past peak. This is not as good a fit as the best Type Ia models, is at odds with the host galaxy redshift prior, and is strongly disfavored by the shape and colors of the SN light curve (see Section 4).

From the preceding analysis, we conclude that HFF14Tom is a Type Ia SN at $z \approx 1.3$. At this redshift, the absorption at $\sim 8700\text{\AA}$ corresponds to the blended Ca II H&K features. This Ca II absorption is commonly seen in Type Ia SN spectra near maximum light, although it is also prominent in the spectra of Type Ib and Ic core collapse SNe (CC SNe). The red color of the HFF14Tom SED is qualitatively consistent with a redshift of $z > 1$ – although this information was not used by SNID for the template matching. As we will see in Section 4, this spectral classification of SN HFF14Tom is reinforced by the photometric information, which also supports classification as a Type Ia SN at $z = 1.3$.

3.2. Spectroscopic Redshift

To refine the redshift and phase constraints on HFF14Tom, we next fit the spectrum with a custom spectral matching program that employs a library of Type Ia SN SEDs. This library is similar to the Type Ia spectral set used by SNID, but also includes more recent SNe with well-observed spectral time series that extend to rest-frame UV wavelengths (e.g. SN 2011fe and 2014J). We first use an approach similar to the SNID algorithm: warping the pseudo-continuum of each template spectrum by dividing out a 3rd-order polynomial to match the observed SED of SN HFF14Tom. From this analysis we find results that are consistent with the SNID fits: a redshift of $z = 1.31 \pm 0.01$ and a phase of 0 ± 3 rest-frame days. The best-fitting spectral template is the normal Type Ia SN 2012cg, shown in the bottom panel of Figure 3, which has χ^2 per degree of freedom ν equal to 42.1/87.

Finally, we repeat the fitting, but without any warping of the templates to account for differences in the continuum shape. In this iteration we only allow each template SED to be scaled in flux coherently at all wavelengths. As shown in Figure 3, we again find that the HFF14Tom SED can be matched by a normal Type Ia SN (SN 2011fe) at redshift $z = 1.31 \pm 0.01$. Without the continuum warping, an alternative fit also arises: the normal Type Ia SN 2011iv at $z = 0.98 \pm 0.01$. Formally, this match provides a slightly better fit to the unwarped HFF14Tom spectrum, although the fit is notably poor at $\sim 8700\text{\AA}$ where the most significant absorption feature is found. Furthermore, a redshift $z \sim 1$ is at odds with the

host galaxy photo- z (1.5 ± 0.2), and we will see in the following section that the photometric data is incompatible with a normal Type Ia SN at $z \sim 1.0$.

Setting aside the $z \sim 1$ solution, all other template matches provide a consistent redshift constraint of $z = 1.31 \pm 0.01$, regardless of whether the templates are warped to match the SN HFF14Tom continuum shape. The inferred age from these fits is 0 ± 3 rest-frame days from peak brightness, which is also consistent with the observed light curve.

4. PHOTOMETRIC CLASSIFICATION

Relative to other SNe at $z > 1$, the SN HFF14Tom light curve was unusually well sampled at rest-frame ultraviolet wavelengths, due to the rapid cadence of the HFF imaging campaign. These ACS observations therefore provide a tight constraint on the time of peak brightness and the evolution of the SN color. Supplemental observations with the WFC3-IR camera provided critical rest-frame optical photometry, enabling a measurement of the apparent luminosity distance through light curve fitting.

As a check on the spectral classification of SN HFF14Tom (Section 3.1), we independently classified the SN using a Bayesian photometric classifier. We use the `sncosmo` software package⁶ to simulate SN light curves from $z = 0.3$ to 2.3 and evaluate the classification probability using traditional Bayesian model selection (as in Jones et al. 2013; Rodney et al. 2014; Graur et al. 2014; Rodney et al. 2015). In this analysis we represent normal Type Ia SNe with the SALT2 model (Guy et al. 2010), and CCSNe with 42 discrete templates (26 Type II and 16 Type Ib/c) drawn from the template library of the SuperNova Analysis software package (SNANA, Kessler et al. 2009b).⁷ Likelihoods are defined by comparing the observed fluxes to model predictions in all passbands where the model is defined. In practice, this means we exclude the F435W and F606W bands, which are too blue for our models at $z > 0.85$.

The CCSN models have free parameters for date of peak brightness (t_{pk}), amplitude, and redshift (z). Due to the expected impact of gravitational lensing magnification, we do not include any prior on the intrinsic luminosity for any SN sub-class. We also do not assign a prior for the SN redshift. This allows our photometric analysis to provide an independent check on the host galaxy photo- z and spectroscopic redshift (Sections 2 and 3.2).

For Type Ia SNe, the SALT2 model has two additional parameters that control the shape (x_1) and color (c) of the light curve. We use conservative priors here, defined to encompass a range of Type Ia SN shapes and colors that is broader than typically allowed in cosmological analyses (see e.g. Kessler et al. 2009a; Sullivan et al. 2011; Rest et al. 2014). For x_1 the prior is a bifurcated Gaussian distribution with mean $\bar{x}_1 = 0$, dispersion $\sigma_{x_1}^+ = 0.9$ and $\sigma_{x_1}^- = -1.5$. The prior for the color parameter c has $\bar{c} = 0.0$, $\sigma_c^- = 0.08$, and $\sigma_c^+ = 0.54$. The c parameter in SALT2 combines intrinsic SN color and extinction due to dust, so the large red tail of this distribution allows for the possibility of several magnitudes of dust extinction along the HFF14Tom line of sight.

⁶ <http://sncosmo.github.io/>

⁷ Throughout this work we use SNANA v10_35g.

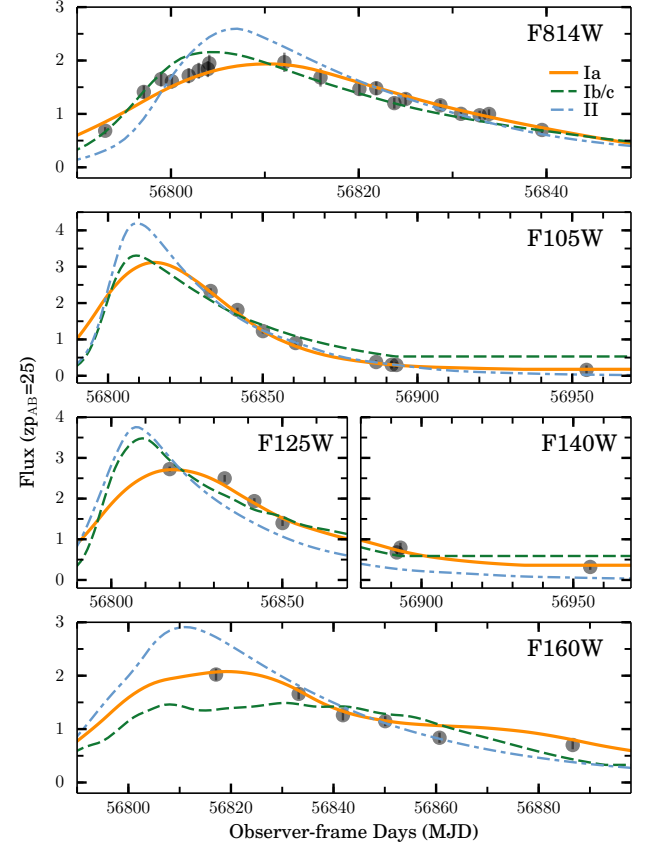


Figure 4. Maximum likelihood model for each SN sub-class, derived from Bayesian model selection using the photometric data alone. Grey points show the observed SN HFF14Tom photometry with error bars, though these are typically smaller than the size of the marker. The Type Ia model (orange solid line) is drawn from the SALT2 template at $z = 1.35$. The best match from all Type Ib/Ic models is based on the Type Ic SN SDSS-14475 at $z = 0.695$ (green dashed line). For the Type II class, the best match is from the Type II-L SN 2007pg at $z = 1.8$ (blue dash-dot line). The Type Ia model is by far the best match, and the only one that is consistent with both the photo- z of the probable host galaxy and the spectroscopic redshift from the SN spectrum.

We also assign a class prior for each of the three primary SN sub-classes (Type Ia, Ib/c, and II), using a fixed relative fraction for each sub-class as determined at $z = 0$ by Smartt et al. (2009) and Li et al. (2011). A more rigorous classification would extrapolate these local SN class fractions to higher redshift using models or measurements of the volumetric SN rate. For simplicity, we do not vary the class priors with redshift, and in practice these priors do not have any significant impact on the resulting classification.

The final photometric classification probability for SN HFF14Tom is $p(\text{Ia}|\mathbf{D}) = 1.0$, with the classification probability from all CCSN sub-classes totaling less than 10^{-32} . The best-fit models for each sub-class are shown in Figure 4, which demonstrates that the CCSN models cannot adequately match the observed photometry. In particular, only the Type Ia model can simultaneously provide an acceptable fit to the well-sampled rising light curve in F814W and the F814W-F160W color near peak.

The marginal posterior distribution in redshift for the Type Ia model is sharply peaked at $z = 1.35 \pm 0.02$,

Table 2
HFF14Tom Distance Modulus and Magnification

Fitter	Redshift	Distance HFF14Tom	Modulus Control	Measured Magnification
SALT2	1.31	44.09 ± 0.16	44.77 ± 0.08	1.87 ± 0.31
SALT2	1.35	44.19 ± 0.16	44.83 ± 0.08	1.80 ± 0.30
MLCS2k2	1.31	44.06 ± 0.09	44.82 ± 0.05	2.01 ± 0.19
MLCS2k2	1.35	44.22 ± 0.09	44.88 ± 0.05	1.83 ± 0.17

which is fully consistent with the photo- z of the presumed host galaxy ($z = 1.5 \pm 0.2$), and $< 2\sigma$ from the spectroscopic redshift of $z = 1.31 \pm 0.01$ derived in Section 3.2. The time of peak brightness is also tightly constrained at $t_{\text{pk}} = 56816.3 \pm 0.3$, which means the spectroscopic observations were collected within 2 rest-frame days of the epoch of peak brightness, consistent with our spectroscopic analysis.

5. LIGHT CURVE FITTING

With the spectroscopic type and redshift securely defined as a normal Type Ia SN at $z = 1.3$, we now turn to fitting the light curve with Type Ia templates to measure the distance modulus. Here we use two independent light curve fitters: the SALT2 model described above and the MLCS2k2 model (Jha et al. 2007).

With both fitters we find light curve shape and color parameters that are fully consistent with a normal Type Ia SN, regardless of whether we adopt the spectroscopic redshift $z = 1.31$ from Section 3.2 or the photometric redshift $z = 1.35$ from Section 4. For SALT2, with the redshift range set to 1.33 ± 0.02 , we find a light curve shape parameter of $x_1 = 0.164 \pm 0.199$ and a color parameter of $c = -0.115 \pm 0.025$, yielding a χ^2 value of 48.4 for 36 degrees of freedom, ν . With the MLCS2k2 fitter the best-fit shape parameter is $\Delta = -0.033 \pm 0.083$ and the color term is $A_V = 0.014 \pm 0.037$, giving $\chi^2/\nu = 23.9/36$.

5.1. Distance Modulus

As in Patel et al. (2014), we derive a distance modulus from the SALT2 fit using⁸

$$\text{dm}_{\text{SALT2}} = m_B^* - M + \alpha(s - 1) - \beta C. \quad (1)$$

Here the parameters for light curve shape s and color C correspond to the SiFTO light curve fitter (Conley et al. 2008), so we first use the formulae from Guy et al. (2010) to convert from SALT2 (x_1 and c) into the equivalent SiFTO parameters. We also add an offset of 0.27 mag to the value of m_B^* returned by SNANA, in order to match the arbitrary normalization of the SALT2 fitter used by Guy et al. (2010) and Sullivan et al. (2011). This conversion allows us to adopt values for the constants M , α , and β from Sullivan et al. (2011), which have been calibrated using 472 SNe from the SNLS3 sample (Conley et al. 2011): $M = -19.12 \pm 0.03$, $\alpha = 1.367 \pm 0.086$, and $\beta = 3.179 \pm 0.101$.

The SNANA version of the MLCS2k2 fitter returns a value for the distance modulus ($\text{dm}_{\text{MLCS2k2}}$) that has

⁸ This avoids confusion by reserving the symbol μ to refer to the lensing magnification. The ‘dm’ is a standard distance modulus, defined as $\text{dm} = 5 \log_{10} d_L + 25$, where d_L is the luminosity distance in Mpc.

an arbitrary zero point offset relative to the SALT2 distances (dm_{SALT2}). To put the two distances onto the same reference frame we add a zeropoint correction of 0.20 mag to the MLCS2k2 distances as in Patel et al. (2014). This correction was derived by applying both fitters to a sample of Type Ia SNe from the SDSS survey (Holtzman et al. 2008; Kessler et al. 2009a), with the extinction law R_V fixed at 1.9.

Final values for the SN distance modulus are shown in Table 2, both for the spectroscopic redshift ($z = 1.31$) and the photometric redshift ($z = 1.35$). The two light curve fitters are consistent within the uncertainties.

5.2. Magnification

To measure the lensing magnification, we would like to avoid introducing systematic uncertainties inherent to any assumed cosmological model (e.g. Nordin et al. 2014). To that end, we follow Patel et al. (2014) and define the magnification by comparing the measured distance modulus of SN HFF14Tom against an average distance modulus derived from a “control sample” of unlensed Type Ia SN at similar redshift. This allows us to make only the minimal assumption that the redshift-distance relationship for Type Ia SN is smooth and approximately linear over a small redshift span, which should be true for any plausible cosmological model.

The unlensed sample comprises 18 spectroscopically confirmed Type Ia SNe in the range $1.14 \leq z \leq 1.42$ from the GOODS and SCP surveys,⁹ which used the HST Advanced Camera for Surveys (Riess & Livio 2006; Suzuki et al. 2012). Using the SALT2 and MLCS2k2 fitters as described above, we get distance modulus measures for every object in this control sample. We then fit a linear relationship for distance modulus vs. redshift, and derive a prediction for the distance modulus of a normal Type Ia SN at the redshift of SN HFF14Tom (Figure 6). This predicted value is given in Table 2 under the “Control” column. The difference between the observed distance of SN HFF14Tom and this control sample value is attributed to the magnification from gravitational lensing:

$$\text{dm}_{\text{control}} - \text{dm}_{\text{HFF14Tom}} = 2.5 \log_{10} \mu. \quad (2)$$

This inferred magnification is reported in the final column of Table 2.

5.3. Comparison to Model Predictions

1) All of the lens models predict a higher magnification than we observe, some with discrepancies > 5 sigma. This suggests a systematic bias inherent to all the models – at least for this particular line of sight.

2) the addition of new lensing constraints from the HFF data does not reduce the tension. From both of the most recent models (Jauzac+ 2014 and Lam+ 2014) the predicted magnification is still significantly higher than the observed.

3) The pre-HFF models that come closest to matching the observed magnification are the Zitrin-NFW and Merten models (also the Williams model, though it has very large uncertainties). Those happen to be two models that relax or remove the assumption of light-traces-mass.

⁹ GOODS: Great Observatories Origins Deep Survey, PI:Giavalisco, HST-PID:; SCP: Supernova Cosmology Project, PI:Perlmutter

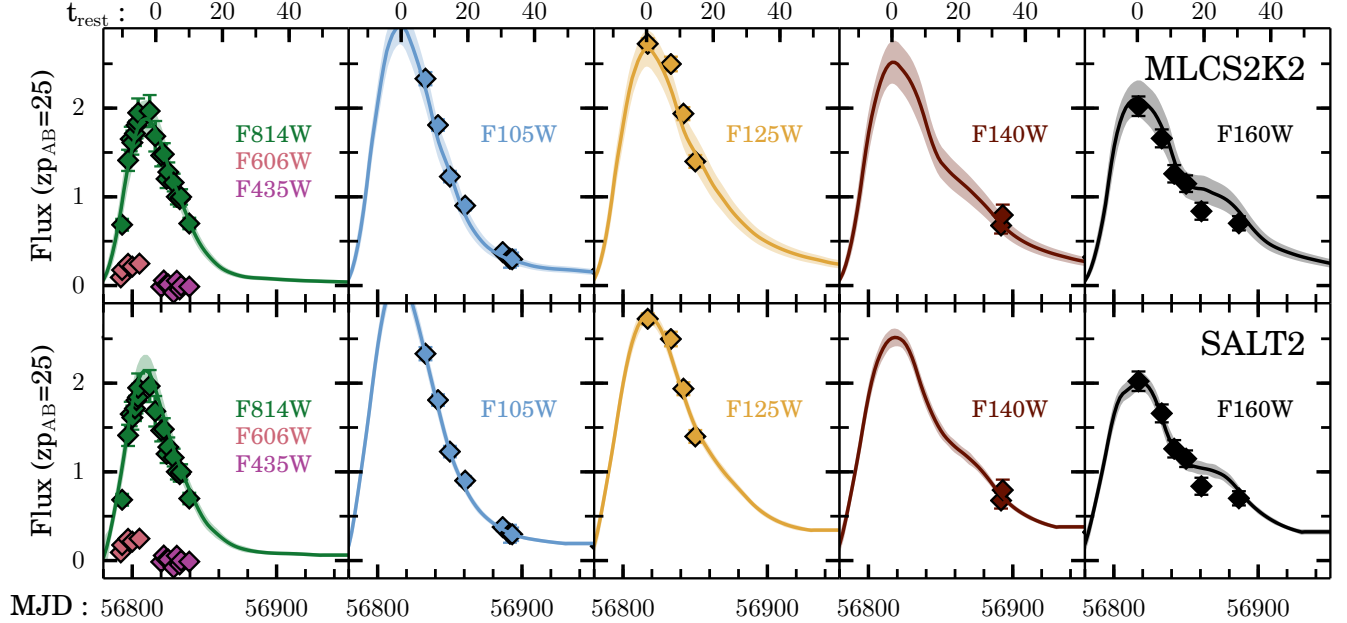


Figure 5. Type Ia light curve fits to SN HFF14Tom using the MLCS2k2 (top row) and SALT2 (bottom row) fitters. The model redshifts are set to $z = 1.33 \pm 0.02$, encompassing both redshift values as determined from spectroscopic and photometric constraints. Solid lines denote the best-fit model and shaded lines show the range allowed by $1-\sigma$ uncertainties on the model parameters. Observed fluxes are shown as diamonds, scaled to an AB magnitude zero point of 25. Error bars are plotted, but most are commensurate with the size of the points. The left-most panel includes observations in the F435W and F606W filters, although these were not used for the fit, as they are bluer than the minimum wavelength for the model. The lower axis marks time in observer frame days, while the top axis shows the time in the rest frame relative to the epoch of peak brightness.

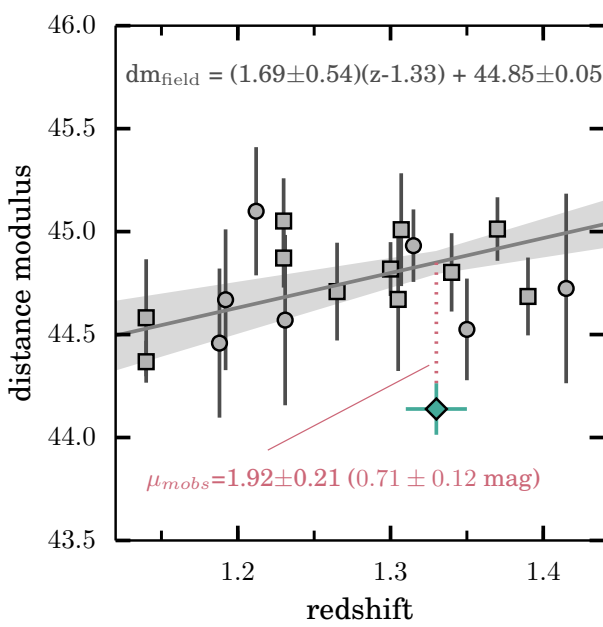


Figure 6. Measurement of the lensing magnification from comparison of the HFF14Tom distance modulus to a sample of unlensed field SN. The distance modulus for each SN is derived from light curve fits using the SALT2 fitter (top panel) and the MLCS2k2 fitter (right).

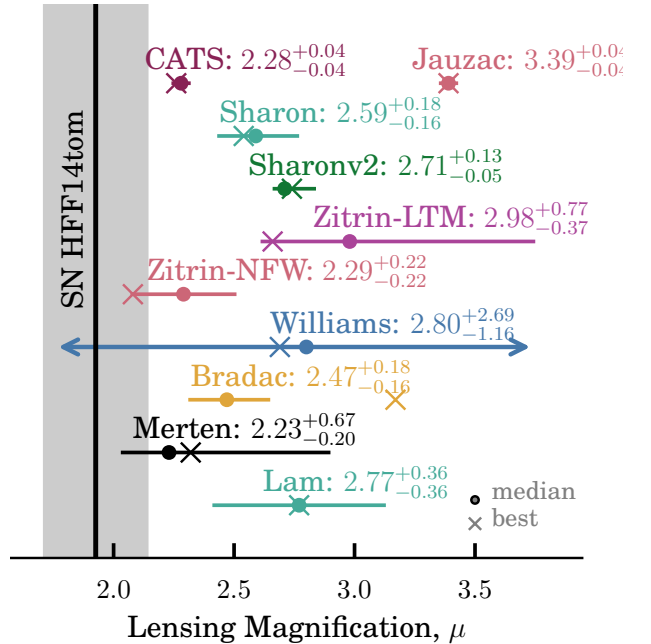


Figure 7. Comparison of the observed lensing magnification to predictions from lens models.

6. DISCUSSION

Possible sources for the bias.

Implications for the systematic error budget of high- z lenses.

Design elements for a survey to build a bigger sample : HST GO, Snapshot, ground-based.

Acknowledgments:

We are very pleased to thank the Hubble Frontier Fields team at STScI for their substantial efforts to make the HFF program successful. In particular, thanks are due to Matt Mountain for the allocation of discretionary orbits for the HFF program; to Jennifer Lotz, Norman Grogin and Patricia Royle for accommodations in strategy and implementation to make the FrontierSN program possible; and to Dan Coe for curating the excellent and accessible lens model comparison tools. We also must thank the CLASH team, led by Marc Postman, for observations, catalogs, and high level science products that were of significant value for this analysis.

Financial support for this work was provided by NASA through grants HST-HF-51312 and HST-GO-13386 from the Space Telescope Science Institute, which is operated by Associated Universities for Research in Astronomy, Inc., under NASA contract NAS 5-26555. Support for this research at Rutgers University was provided in part by NSF CAREER award AST-0847157 to SWJ. The Dark Cosmology Centre is supported by the Danish National Research Foundation.

Facilities: HST (WFC3)

REFERENCES

Benítez, N. 2000, ApJ, 536, 571

- Blondin, S., & Tonry, J. L. 2007, ApJ, 666, 1024
 Coe, D., et al. 2013, ApJ, 762, 32
 Conley, A., et al. 2011, ApJS, 192, 1
 —. 2008, ApJ, 681, 482
 Fruchter, A. S., et al. 2010, in STSCI Calibration Workshop Proceedings, Baltimore, MD, 21-23 July 2010, ed. S. D. . C. Oliveira (Space Telescope Science Institute), 376
 Goobar, A., et al. 2009, A&A, 507, 71
 Graur, O., et al. 2014, ApJ, 783, 28
 Guy, J., et al. 2010, A&A, 523, A7
 Holtzman, J. A., et al. 2008, AJ, 136, 2306
 Jha, S., Riess, A. G., & Kirshner, R. P. 2007, ApJ, 659, 122
 Jones, D. O., et al. 2013, ApJ, 768, 166
 Kessler, R., et al. 2009a, ApJS, 185, 32
 —. 2009b, PASP, 121, 1028
 Landsman, W. B. 1993, in Astronomical Society of the Pacific Conference Series, Vol. 52, Astronomical Data Analysis Software and Systems II, ed. R. J. Hanisch, R. J. V. Brissenden, & J. Barnes, 246
 Li, W., et al. 2011, MNRAS, 412, 1441
 Liu, Y., & Modjaz, M. 2014, arXiv:1405.1437
 Nordin, J., et al. 2014, MNRAS, 440, 2742
 Patel, B., et al. 2014, ApJ, 786, 9
 Rest, A., et al. 2014, ApJ, 795, 44
 Riehm, T., et al. 2011, A&A, 536, A94
 Riess, A. G., & Livio, M. 2006, ApJ, 648, 884
 Rodney, S. A., et al. 2014, AJ, 148, 13
 —. 2015, submitted to AJ;
 (pdf at <http://bit.ly/10Zmk1X>)
 Smartt, S. J., et al. 2009, MNRAS, 395, 1409
 Stetson, P. B. 1987, PASP, 99, 191
 Sullivan, M., et al. 2011, ApJ, 737, 102
 Suzuki, N., et al. 2012, ApJ, 746, 85
 Zheng, W., et al. 2012, Nature, 489, 406